SCIENCE CHINA
Information Sciences

• RESEARCH PAPER •
Special Topic: Two-Dimensional Materials and Device Applications

June 2023, Vol. 66 160407:1–160407:9
https://doi.org/10.1007/s11432-023-3762-9

Growth of uniformly doped black phosphorus films through versatile atomic substitution

Cheng CHEN[1,2], Yang LU[2,3], Chang LI[2], Xingang HOU[2], Yongjie WANG[2,3], Junrong ZHANG[1,2], Junyong WANG[2] & Kai ZHANG[2*]

[1]*School of Nano-Tech and Nano-Bionics, University of Science and Technology of China, Hefei* 230026*, China;*
[2]*CAS Key Laboratory of Nanophotonic Materials and Devices & Key Laboratory of Nanodevices and Applications, i-Lab, Suzhou Institute of Nano-Tech and Nano-Bionics, Chinese Academy of Sciences, Suzhou* 215123*, China;*
[3]*Nano Science and Technology Institute, University of Science and Technology of China, Suzhou* 215123*, China*

Received 2 March 2023/Revised 24 March 2023/Accepted 6 May 2023/Published online 18 May 2023

Abstract For the emerging excellent two-dimensional semiconductor black phosphorus (BP), doping has been proven as an effective way to tune its intrinsic properties. For the further development and expansion of BP-based research and application, the direct growth of doped BP films is highly desirable but still remains a challenge. In this work, the direct growth of uniformly doped-BP films on silicon substrates is achieved by a simple one-step vapor growth. The proposed decoupled feeding strategy significantly improves the effectiveness of doping and enables uniform dopant distribution in the grown films. The substitutional doping nature and high crystal quality of the grown doped films are confirmed by microscopy and crystal structural determination. Electrical transport measurement results reveal that Se and Te dopants perform mild electron doping effect and enable improve the electron mobility relative to pristine BP, while As dopant performs mild hole doping effect. It is believed that the direct growth of doped BP films in this work will facilitate the research development of BP in electronics and optoelectronics.

Keywords black phosphorus, dope, vapor growth, thin film, two-dimensional materials

Citation Chen C, Lu Y, Li C, et al. Growth of uniformly doped black phosphorus films through versatile atomic substitution. Sci China Inf Sci, 2023, 66(6): 160407, https://doi.org/10.1007/s11432-023-3762-9

1 Introduction

As a fascinating elemental two-dimensional (2D) material, black phosphorus (BP) has attracted huge interest since its rediscovery in 2014 [1]. It possesses high carrier mobility (up to 1000 $cm^2 \cdot V^{-1} \cdot s^{-1}$), widely tunable direct bandgap (from 0.3 to 2.0 eV) and characteristic in-plane anisotropy [2–4]. For these unique properties, BP has promising potential applications in next-generation electronics and optoelectronics [4–9]. To develop and broaden BP-based studies and applications, controllable modification of physical and chemical properties such as ambient stability and transport behavior is of great importance. As the cornerstone of semiconductor technology, doping has been widely used to tune the inherent properties of conventional semiconductors and some 2D layered materials such as graphene and MoS_2 [10–12]. In recent years, various doping strategies for BP have been developed utilizing a range of methods, such as mechanical exfoliation from the doped-bulk crystals [13, 14], post-vapor deposition doping [15, 16], and electrostatic carrier doping [17], to name a few. These doping methods require multi-step processes include such as exfoliation and post-treatments, which are valid but usually complicated and unfavorable for further device application. In this regard, direct growth of doped BP films on substrates seems preferable but has thus far remained a challenge despite several preliminary explorations [18, 19]. The difficulty for directly growing doped BP films possibly arises from unmatched precursors feeding rate of P_4 and dopant during the growth process.

Herein, we report the direct growth of high-quality doped-BP film on SiO_2 substrates using a simple one-step vapor growth process, the dopant elements can include Se, Te, and As atoms. The as-grown

* Corresponding author (email: kzhang2015@sinano.ac.cn)

doped BP films exhibited highly homogeneous dopant distribution, which benefited from better feeding control realized by the decoupled feeding strategy. Microscopy and crystal structural determination reveal the substitutional doping nature and high crystal quality of the as-grown doped films. Electrical transport measurement results demonstrate that Se and Te dopants perform a mild hole doping effect and improve the electron mobility compared with pristine BP, while As dopant performs a mild hole doping effect and degrades the electronic performance.

2 Results and discussion

To grow the doped BP film, a furnace with one uniform heating zone was employed, the setup schematics are shown in Figure 1(a). The starting materials include dopant precursors (Se powders, TeI_4 powders, and gray As particles), red P particles, Sn powders, and SnI_4 particles, which are mixed and enclosed in an evacuated quartz ampoule. Firstly, the ampoule is heated up to 970 K within 3 h, and then cooled to 770 K within 3 h. After holding at 770 K for 6 h, the ampoule is cooled to room temperature for 12 h. It is believed that temperature fluctuation is not suited to grow high-quality and uniformly doped BP film, so the spatial temperature gradient was avoided as far as possible throughout the growth process, similar to the previous report about the growth of BP bulk crystal [20, 21]. In this work, the tube furnace can be replaced by a muffle furnace to simplify the experiment and enhance yield.

It is noted that the partial pressure of the dopant precursors is low than that of P precursors, which results in a lower feeding rate of the dopant element than that of P_4 as well. If the dopant precursors feeding was inadequate under a mass of P_4 feeding during the fast film growth process, the dopant amount in the grown film will be significantly limited. So the challenge for the growth of doped BP film was how to control the feeding rate of P precursors and dopant precursors. In view of the above consideration, we design the setup for the growth of the doped BP film as schematically shown in Figures 1(a) and (b). The growth system was divided into two chambers which were connected by a flow restrictor, similar to the previously reported multi-tube vapor growth system [22]. This flow restrictor could be a simple capillary channel as shown in Figure 1(a). The dopant precursors were evenly spread beneath the substrate to supply sublimated dopant feeding as much as possible. While the P precursors were placed in another chamber, the sublimated P_4 vapor will diffusion to the substrate surface through a capillary channel. The transport rate of P precursors (N) can be described by the following equation [23]:

$$N = \frac{\pi d^4}{16\eta l R}\left(\frac{P_s^2 - P_g^2}{T}\right), \tag{1}$$

where d and l are the radius and length of the capillary channel; η is the viscosity of the P_4 vapor; P_s and P_g are the P_4 pressure at the source and crystal growth chamber, respectively; T is the absolute temperature; R is the universal gas constant. Based on the above relation, through optimizing the growth parameters including capillary channel radius d and the distance between the substrate and dopant precursors, the P precursors feeding rate can be well controlled to match well with the dopant precursor sublimation rate, as shown in Figure 1(b).

Using this proposed growth strategy, BP film doped with Te, Se, and As can be directly grown on SiO_2 substrate, as shown in Figures 1(c)–(e). In this work, the grown doped BP films usually present a trapezoidal shape similar to the previously reported grown BP flakes [19, 24, 25], and the lateral size usually ranges from 50 μm to 1 mm (Figure S1). Besides, the thickness of the as-grown doped BP films usually ranges from 10 to 300 nm (Figure 1(f)).

Furthermore, micro-Raman spectroscopy was utilized to identify and characterize the grown doped BP film, the compared Raman spectrum was shown in Figure 1(g). The three distinct characteristic Raman peak located at ∼362.2, 439.4, and 466.5 cm^{-1} was corresponding to A_g^1, B_{2g}, and A_g^2 vibration modes of crystalline BP, respectively [26, 27]. In comparison with the pristine BP film, it can be observed that the Raman peak of the doped BP film redshifted more or less. Moreover, for Te-doped BP films and Se-doped BP films, two new Raman peaks emerged at 194.2 and 230.1 cm^{-1} (Figure 1(h)). Similar to that of doped-bulk crystal, which belongs to the edge phonon vibrational modes (B_g^1 and B_{3g}^1) of BP crystal according to the previous report [21, 27, 28]. We proposed the possible reason is that the introduced doped atoms break the symmetry of the crystal structure, further activating both edge phonon vibration modes. For As-doped BP films, the new Raman peaks appeared at 200–300 cm^{-1} regime and 300–380 cm^{-1} regime owing to the introduced As–As bonds and As–P bonds as the previous report, respectively [13].

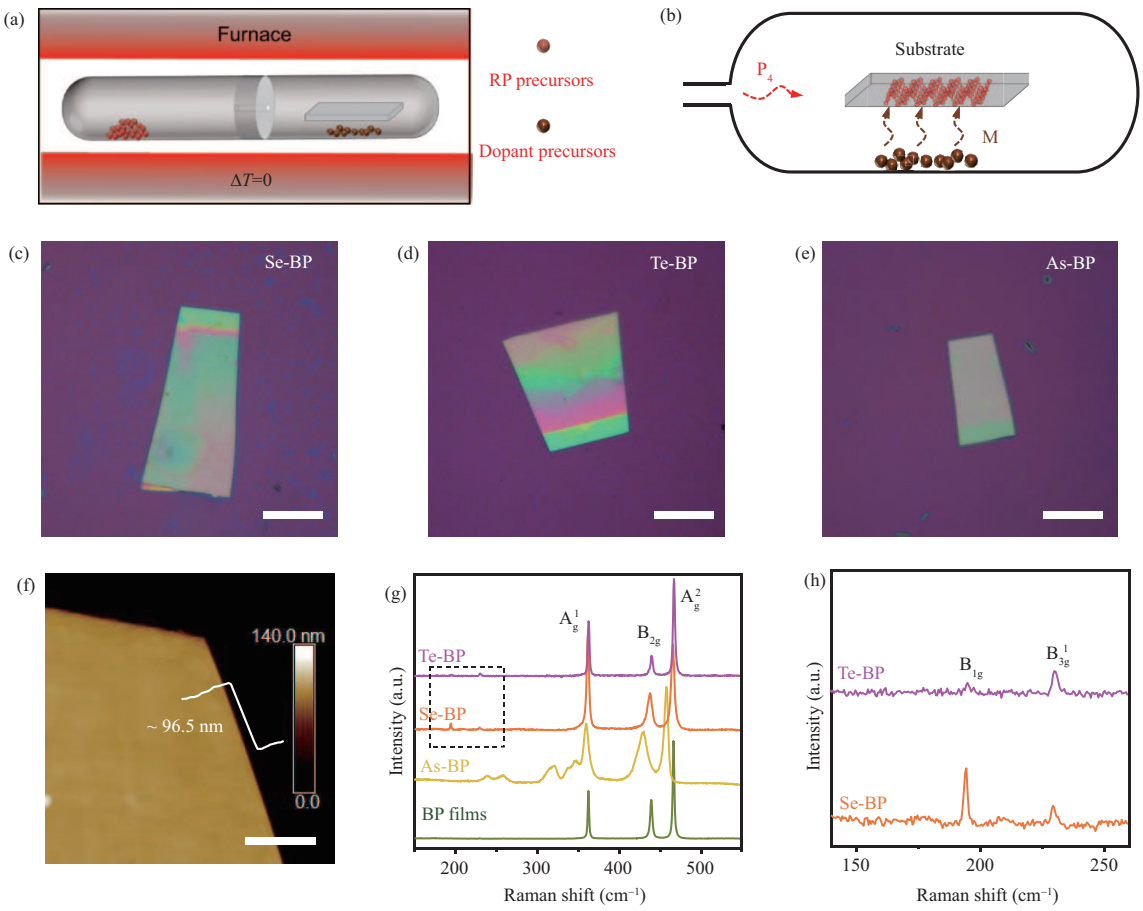

Figure 1 (Color online) Modified vapor transport growth of doped BP films and corresponding optical images. (a), (b) Schematic diagram for decoupled feeding growth of doped BP films on substrates. (c)–(e) Typical optical images of the as-grown Se-doped, Te-doped, and As-doped BP films on Si/SiO_2 substrate, scale bar is 50 μm. (f) A typical atomic force microscope (AFM) image of a grown film, scale bar is 10 μm. (g), (h) Compared Raman spectrum of the as-grown doped BP films.

To test the effect of the proposed decoupled feeding route for the growth of doped BP films, compared experiments were carried out for the growth with and without this strategy, here we take the growth of As-doped BP film as an example. As shown in Figures 2(a) and (b), if As powders and P powders were directly mixed as precursors in the ampule, the As dopant amount in the grown film was about 9.6% measured by X-ray photoelectron spectroscopy (XPS) (Figure 2(c)). Under the same experimental condition (including precursors amount and proportion, temperature parameter, and quartz ampoule parameter), if we adopt the decoupled feeding route, a high As dopant concentration of up to 18.5% atomic ratio was achieved (Figure 2(d)). This result verifies that our proposed feeding route can significantly promote atomic doping during film growth, as previously mentioned. Moreover, element distribution mapping measured by XPS was further used to compare the doping homogeneity with the two-type feeding method. As shown in Figures 2(e) and (f), element distribution in films was clearly visible through color contrast, which demonstrates that the doped BP films grown by the proposed feeding route possess higher element distribution uniformity than that grown by the common strategy. The possible reason for this result is that P4 flow in the decoupled feeding route is tractable and makes for a stable dopant feeding condition, which was in favor of a more homogeneous dopant distribution.

In addition to the As-doped BP films, we also conducted the XPS and energy dispersive X-ray (EDX) measurements on the Se-doped and Te-doped BP films to investigate the doping effect. As shown in Figure 3, a surface area with a beam size of 250 μm × 250 μm on the sample was selected randomly to characterize the dopant element peak and corresponding element distribution mapping. The result visually revealed the undoubted existence of Se and Te energy spectrum peaks in the as-grown films, and the dopant element exhibited a highly homogeneous distribution. Both the Se $3d_{5/2}$ and Te $3d_{5/2}$ element energy peaks (at 573.9 and 55.2 eV, respectively) slightly shift toward the higher binding energy compared with both that of Te and Se in zero valence state (573.0 and 55.1 eV, respectively), which indicate the

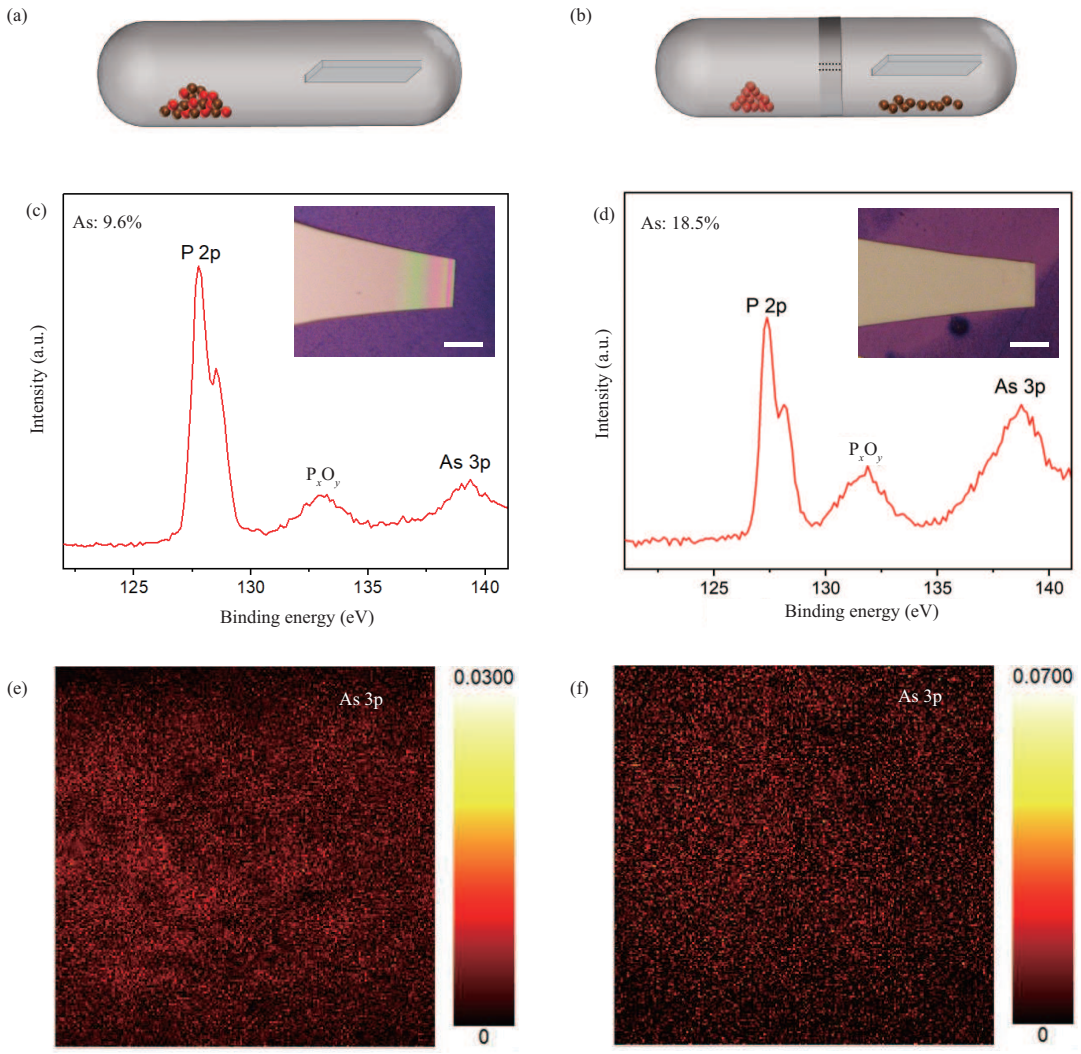

Figure 2 (Color online) Comparison of As-doped BP films grown through decoupled feeding route and common feeding route. (a), (b) Schematic diagrams for decoupled feeding route and common feeding route. (c), (d) XPS core-level spectra of P 2p and As 3p. Inset: optical images of measured samples grown from two different feeding routes. (e), (f) Element mappings extracted from the intensity of the As 3d peak, the XPS spectra were measured based on the samples shown in the inset of (c) and (d), respectively. Scale bar is 50 μm.

existence form of the dopant atoms should belong to chemical bond element inside the crystal rather than elementary deposition on the film surface. Besides, a series of EDX element mapping measurements have also been performed to prove the success of growing uniformly doped BP films (Figures S2 and S3). These results convincingly verified the universality and effectiveness of our proposed strategy for the growth of uniformed doped BP films. Moreover, based on the peak intensity of the dopant element and P element, the highest dopant atomic ratio of 0.8%, 0.4%, and 70% can be calculated for Se-doped, Te-doped film, and As-doped film, respectively. Actually, we have tried the growth of Bi-doped BP films and Sb-doped BP films, but unfortunately, we have not detected the existence of these dopant elements in the obtained BP films. The possible reason is that the high sublimation temperature and large atomic radius of Sb and Bi hinder their doping process.

Although some previous studies about the growth of doped BP bulk crystal have given the doped crystal structural model as shown in Figure 4(a) [13,29,30], the doping type (interstitial type or substituted type) and atoms distribution in doped BP crystal lattice have not been well demonstrated by corresponding characterizations. In this regard, we employed X-ray diffraction patterns (XRD) to study the crystal structure of the as-grown doped BP film. As shown in Figure 4(b), all diffraction peaks of the doped BP films can be indexed with (0 2n 0), which was the normal stack direction of the orthorhombic structure, similar to BP crystal (A17 type structure). This result indicated that these dopant atoms

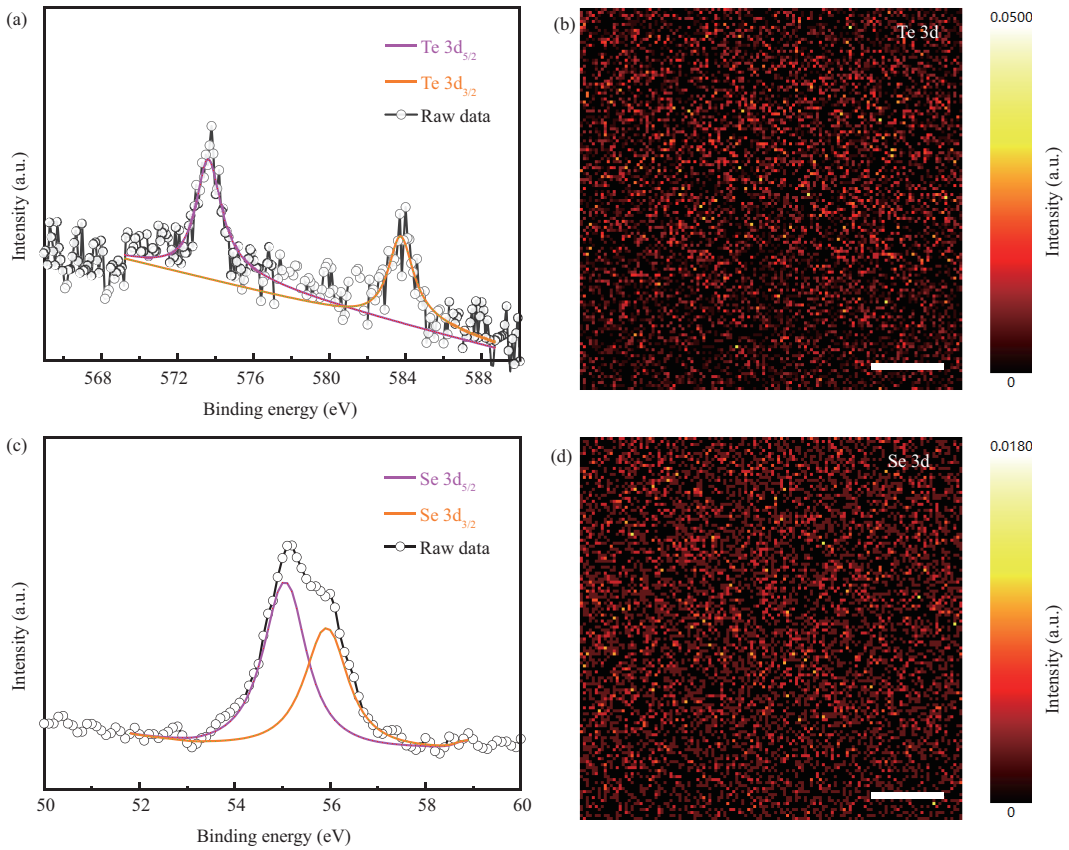

Figure 3 (Color online) (a), (b) XPS core-level spectra of Te 3d and corresponding element mapping measured on a Te-doped BP film, scale bar is 50 μm; (c), (d) XPS core-level spectra of Se 3d and corresponding element mapping measured on a Se-doped BP film, scale bar is 50 μm.

in films do not change the characteristic BP lattice structure. It was also observed that the diffraction peak downshift and broaden for the doped BP films, which indicated the crystal lattice expand after the introduction of the dopant atoms with a larger radius, and the lattice expansion will intensify with the dopant amount increased (Figures 4(c) and S4). In addition, all XRD measurements of doped BP films show only one set of diffraction peaks without other crystalline phase residues, indicating no phase separation occurred in the doped BP films. In order to further investigate the microscopic crystal structure and atomic distribution in the doped BP film, high-angle annular dark-field-scanning transmission electron microscopy (HAADF-STEM) was performed based on the samples obtained from the wet-transfer technique. Figures 4(d)–(f) show the atoms arrangement of Te-doped, Se-doped, and As-doped BP films, respectively, which were viewed along the [010] zone axis as shown in Figure 4(a). The dopant atoms (brighter sites) and P atoms (darker sites) can be clearly discriminated based on the difference in the atomic numbers. This result unambiguously verified the existence of dopant atoms inside the crystal lattice once again. The corresponding intensity line profile obtained along the armchair direction was shown in Figures 4(g)–(i). It should be noted that no lattice distortion and interstitial atoms can be observed, which indicated the dopant atoms are exactly substitution in the crystal lattice, matching well with the aforementioned XRD measurement results.

It is known that BP suffers from poor ambient stability, which hinders its practical application. Here, we investigated the ambient stability of the as-grown pristine and doped BP films utilizing AFM characterization and optical microscope observations. As shown in Figures 5 and S5, the result shows that Se, Te, and As doped BP films all exhibit different degrees of improved ambient stability compared with that of pristine BP. Particularly, As-doped BP samples (b-$As_{0.7}P_{0.3}$) can maintain almost unchanged surface topography after ambient exposure for 6 days, indicating its significant improvement in ambient stability, this result was different from the previous report. The possible reason is that As dopant makes BP more hydrophobic and thus inhibits its further degradation [26, 31], because we found that the viscosity (amount of water absorbed) of As-doped BP films surface was significantly smaller than pristine BP films

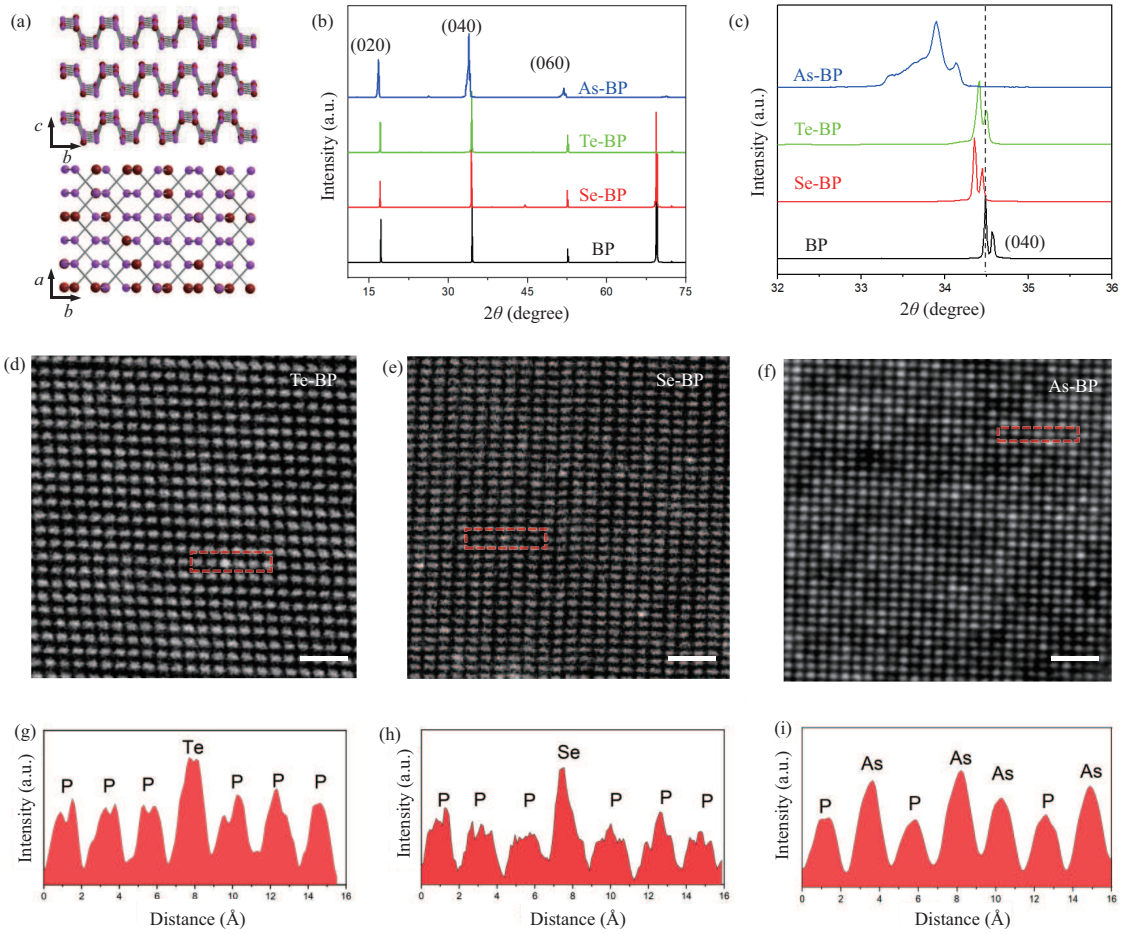

Figure 4 (Color online) (a) Side and top views of the orthorhombic structure of substitution-doped BP crystal. (b) XRD patterns of the as-grown Se-doped, Te-doped, and As-doped BP films (b-$As_{0.5}P_{0.5}$). (c) Enlarged (040) diffraction peaks of the films, indicate that the diffraction peak downshift and broaden of the doped BP films compared with pristine BP films. (d)–(f) HAADF-STEM images of Te-doped, Se-doped, and As-doped BP, the brighter locations are the dopant substituted sites. Scale bar is 1 nm. (g)–(i) Intensity profiles along the red box shown in (d)–(f), respectively.

during the AFM measurement process.

It is known that doping is widely used to adjust the electronic transport of conventional semiconductors. To investigate the effect of doping on the electrical properties of the as-grown doped BP film, back-gate field effect transistors (FETs) were fabricated based on the doped BP films (see Figures 6(a) and (b)). The AFM measurement and corresponding height profiles were demonstrated in Figure S6, indicating the pristine and doped BP channels have similar thicknesses. Figure 6(c) shows the compared output curves (I_{ds}-V_{ds}) of pristine BP film and doped BP films, the near linear shape indicated the good Ohmic contact between the electrode and channel. Figure 6(d) shows the compared transfer curves (I_{ds}-V_g) for the several kinds of doped BP films and pristine BP films, all of those exhibit typical hole-dominated ambipolar transport behavior. From the linear extrapolation of the linear region of the hole and electron side, the threshold voltage V_{th} can be extracted, and the hole concentration can be further estimated, as shown in Figure S7. It was found that the hole concentration of Se-doped BP and Te-doped BP decreased compared with that of pristine BP, while the hole concentration of As-doped BP was increased compared with that of pristine BP. This result indicated that Te and Se atoms should serve as n-type dopants for BP crystal, and As should serve as p-type dopants for BP crystal. The remarkable n-type doping effect to Te was consistent with the previous report [14, 32], but real n-type dominated transport characteristic of Te-doped BP has not been observed, possibly due to the low Te dopant amount.

Similarly, extracted from the linear regime of the transfer curve, the field effect carrier mobility of the

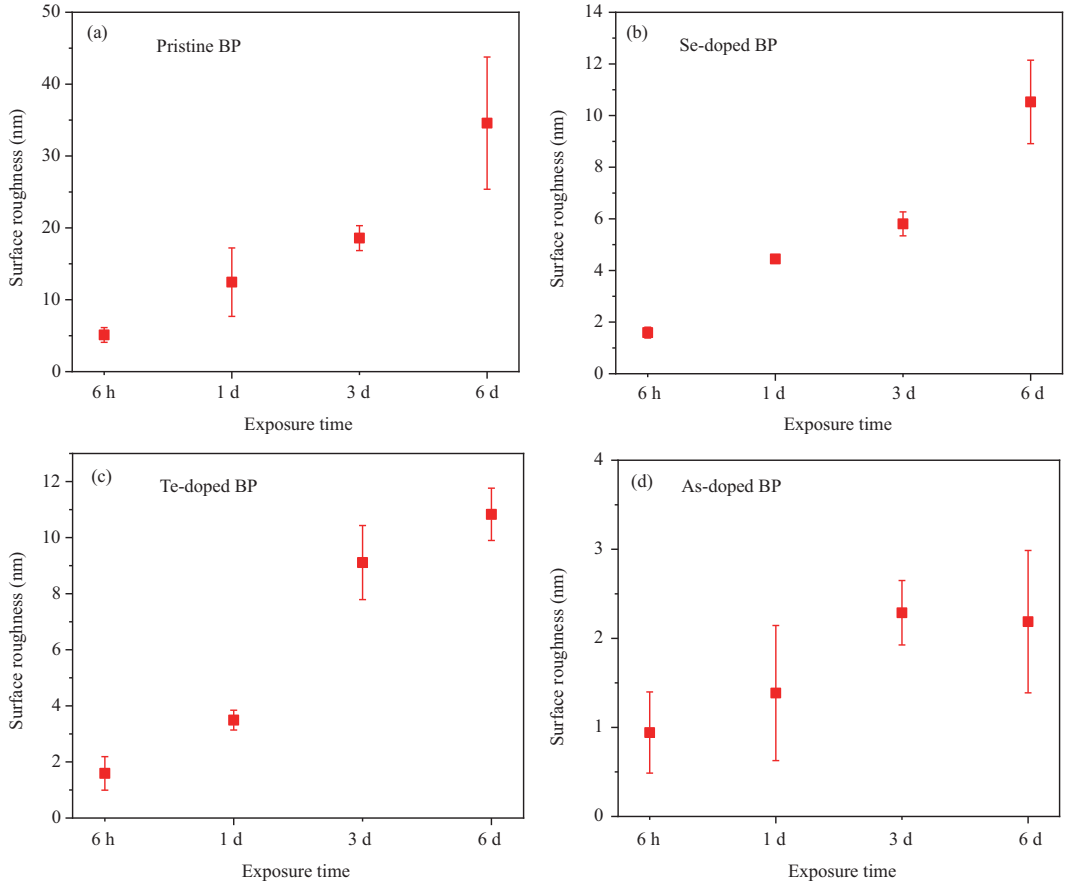

Figure 5 (Color online) Evolution of the surface roughness with increasing exposure time (6 h, 1 day, 3 days, and 6 days) for pristine (a), Se-doped (b), Te-doped (c), and As-doped (d) BP samples, respectively. The corresponding AFM images are shown in Figure S5. Each sample we selected had a similar thickness (∼28 nm) and was exposed to the same conditions. The error bars represent the standard deviations of surface roughness from 4 measured areas.

devices can be estimated using the following formula:

$$\mu = \frac{\mathrm{d}I_{\mathrm{ds}}}{\mathrm{d}V_g} \cdot \frac{L}{WC_{\mathrm{ox}}V_{\mathrm{ds}}}, \tag{2}$$

where $\mathrm{d}I_{\mathrm{ds}}/\mathrm{d}V_g$ denotes the maximum slope of the linear region in the transfer curve; L and W are the length and width of the channel materials, respectively; C_{ox} is the back gated capacitance per unit area. For the devices shown in Figure 6(d), the hole and electron mobility can be calculated from the hole and electron side of the transfer curve, respectively. The average hole mobility of Se-doped BP and Te-doped BP was about 430 and 433 $\mathrm{cm^2{\cdot}V^{-1}{\cdot}s^{-1}}$, similar to that value of pristine BP (441 $\mathrm{cm^2{\cdot}V^{-1}{\cdot}s^{-1}}$). Noteworthily, the average electron mobility of Se-doped BP and Te-doped BP was about 5.8 and 11.7 $\mathrm{cm^2{\cdot}V^{-1}{\cdot}s^{-1}}$, distinctly higher than that value of pristine BP (1.5 $\mathrm{cm^2{\cdot}V^{-1}{\cdot}s^{-1}}$), the possible reason was that the charge (electron) trapping sites were filled by the electron provided from the Se and Te dopant, which relieve the trapped charge scattering [15]. For the As-doped BP device, the calculated hole mobility of 303 $\mathrm{cm^2{\cdot}V^{-1}{\cdot}s^{-1}}$ was distinctly lower than that of the pristine BP device, and its electrons mobility of 0.84 $\mathrm{cm^2{\cdot}V^{-1}{\cdot}s^{-1}}$ was slightly lower than that of pristine BP, which was probably due to the increased scattering derived from an amount of As dopant. It is also found that the degradation of mobility will intensify with the dopant amount increasing, but the lowest hole mobility is still above 250 $\mathrm{cm^2{\cdot}V^{-1}{\cdot}s^{-1}}$ (Figure 6(f)).

In summary, large-scale doped BP films (Se-doped, Te-doped, and As-doped) have been directly grown on SiO_2 substrate by a simple one-step vapor growth method. Benefiting from the better control on the feeding, the grown doped BP films display a highly homogeneous distribution, which is evidenced by XPS and EDX. The as-grown doped BP films retain the orthorhombic crystalline similar to BP and the dopant atoms are substituted distribution in the crystal lattice, as demonstrated by XRD and STEM

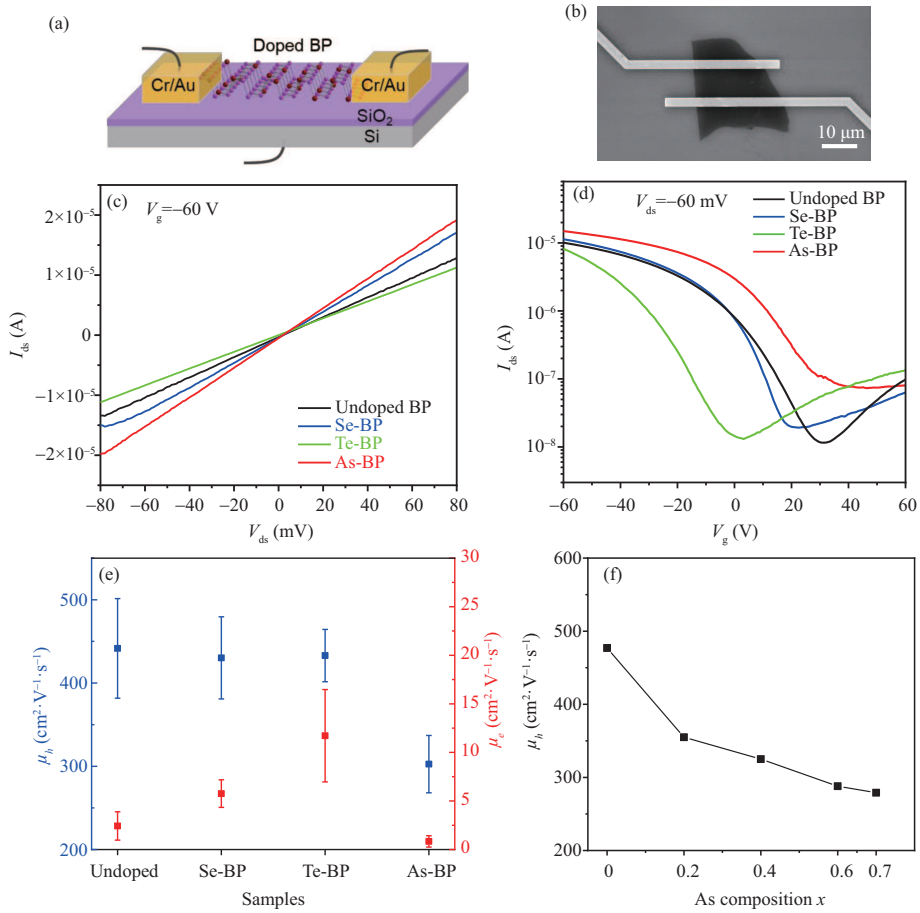

Figure 6 (Color online) (a) Schematic of the doped BP FET fabricated on a SiO_2 (300 nm)/Si back gated substrate, with Cr/Au (10 nm/70 nm) as the electrodes. (b) A typical SEM image of the FET device fabricated used As-doped BP as the channel. (c) Compared output characteristic curves acquired with V_g of −60 V and V_{ds} from −80 to 80 mV, the channels materials are undoped, Se-doped, Te-doped, and As-doped BP films (b-$As_{0.4}P_{0.6}$), respectively. (d) Compared transfer characteristics curves on logarithmic scales at a fixed bias of V_{ds} = 60 mV. (e) Calculated field effect mobility of the various doped BP samples. The error bars represent the standard error from 5 samples. (f) Calculated field effect hole mobility of As-doped BP (b-As_xP_{1-x}) versus As composition x.

measurements. Furthermore, electrical transport studies revealed that Se and Te doped BP films exhibit mild electron doping effects and higher electron mobility relative to pristine BP films, while As-doped BP films exhibit mild hole doping effects and degraded electrical properties. In this work, it was envisioned that the proposed method for the direct growth of doped BP films will facilitate the research development of BP family materials in electronics and optoelectronics.

Acknowledgements This work was supported by National Key Research and Development Program of China (Grant No. 2021YFA1200804), National Natural Science Foundation of China (Grant Nos. 62274175, 61927813), and Jiangsu Province Key R&D Program (Grant No. BE2021007-3). We thank Zhiyun LI for analyzing the XPS measurement results. The support from the Vacuum Interconnected Nanotech Workstation (Nano-X) of Suzhou Institute of Nano-tech and Nano-bionics (SINANO), Chinese Academy of Sciences is also acknowledged.

Supporting information Figures S1–S7. The supporting information is available online at info.scichina.com and link.springer.com. The supporting materials are published as submitted, without typesetting or editing. The responsibility for scientific accuracy and content remains entirely with the authors.

References

1 Li L, Yu Y, Ye G J, et al. Black phosphorus field-effect transistors. Nat Nanotech, 2014, 9: 372–377
2 Liu H, Neal A T, Zhu Z, et al. Phosphorene: an unexplored 2D semiconductor with a high hole mobility. ACS Nano, 2014, 8: 4033–4041
3 Ling X, Wang H, Huang S, et al. The renaissance of black phosphorus. Proc Natl Acad Sci USA, 2015, 112: 4523–4530
4 Castellanos-Gomez A. Black phosphorus: narrow gap, wide applications. J Phys Chem Lett, 2015, 6: 4280–4291
5 Carvalho A, Wang M, Zhu X, et al. Phosphorene: from theory to applications. Nat Rev Mater, 2016, 1: 16061
6 Zhang Y, Wang S, Chen S, et al. Wavelength-tunable mid-infrared lasing from black phosphorus nanosheets. Adv Mater, 2020, 32: 1808319

7 Kim H, Uddin S Z, Lien D H, et al. Actively variable-spectrum optoelectronics with black phosphorus. Nature, 2021, 596: 232–237
8 Youngblood N, Chen C, Koester S J, et al. Waveguide-integrated black phosphorus photodetector with high responsivity and low dark current. Nat Photon, 2015, 9: 247–252
9 Biswas S, Grajower M Y, Watanabe K, et al. Broadband electro-optic polarization conversion with atomically thin black phosphorus. Science, 2021, 374: 448–453
10 Li H, Duan X, Wu X, et al. Growth of alloy $MoS_{2x}Se_{2(1-x)}$ nanosheets with fully tunable chemical compositions and optical properties. J Am Chem Soc, 2014, 136: 3756–3759
11 Wei D, Liu Y, Wang Y, et al. Synthesis of N-doped graphene by chemical vapor deposition and its electrical properties. Nano Lett, 2009, 9: 1752–1758
12 Gao H, Suh J, Cao M C, et al. Tuning electrical conductance of MoS_2 monolayers through substitutional doping. Nano Lett, 2020, 20: 4095–4101
13 Liu B, Köpf M, Abbas A N, et al. Black arsenic-phosphorus: layered anisotropic infrared semiconductors with highly tunable compositions and properties. Adv Mater, 2015, 27: 4423–4429
14 Yang B, Wan B, Zhou Q, et al. Te-doped black phosphorus field-effect transistors. Adv Mater, 2016, 28: 9408–9415
15 Xiang D, Han C, Wu J, et al. Surface transfer doping induced effective modulation on ambipolar characteristics of few-layer black phosphorus. Nat Commun, 2015, 6: 6485
16 Kim D K, Hong S B, Jeong K, et al. P-N junction diode using plasma boron-doped black phosphorus for high-performance photovoltaic devices. ACS Nano, 2019, 13: 1683–1693
17 Xu Y, Yuan J, Zhang K, et al. Field-induced n-doping of black phosphorus for CMOS compatible 2D logic electronics with high electron mobility. Adv Funct Mater, 2017, 27: 1702211
18 Young E P, Park J, Bai T, et al. Wafer-scale black arsenic-phosphorus thin-film synthesis validated with density functional perturbation theory predictions. ACS Appl Nano Mater, 2018, 1: 4737–4745
19 Izquierdo N, Myers J C, Golani P, et al. Growth of black arsenic phosphorus thin films and its application for field-effect transistors. Nanotechnology, 2021, 32: 325601
20 Zhao M, Niu X, Guan L, et al. Understanding the growth of black phosphorus crystals. CrystEngComm, 2016, 18: 7737–7744
21 Liu M, Feng S, Hou Y, et al. High yield growth and doping of black phosphorus with tunable electronic properties. Mater Today, 2020, 36: 91–101
22 Sanghera H K, Cantwell B J, Aitken N M, et al. The growth of CdTe bulk crystals using the multi-tube physical vapour transport system. J Cryst Growth, 2002, 237-239: 1711–1715
23 Abernathey J R, Greenwell D W, Rosenberger F. Congruent (diffusionless) vapor transport. J Cryst Growth, 1979, 47: 145–154
24 Izquierdo N, Myers J C, Seaton N C A, et al. Thin-film deposition of surface passivated black phosphorus. ACS Nano, 2019, 13: 7091–7099
25 Han D, Liu Q, Zhang Q, et al. Synthesis of highly crystalline black phosphorus thin films on GaN. Nanoscale, 2020, 12: 24429–24436
26 Favron A, Gaufrés E, Fossard F, et al. Photooxidation and quantum confinement effects in exfoliated black phosphorus. Nat Mater, 2015, 14: 826–832
27 Ribeiro H B, Pimenta M A, de Matos C J S. Raman spectroscopy in black phosphorus. J Raman Spectrosc, 2018, 49: 76–90
28 Ribeiro H B, Villegas C E P, Bahamon D A, et al. Edge phonons in black phosphorus. Nat Commun, 2016, 7: 12191
29 Zhang Z, Khurram M, Sun Z, et al. Uniform tellurium doping in black phosphorus single crystals by chemical vapor transport. Inorg Chem, 2018, 57: 4098–4103
30 Antonatos N, Bouša D, Shcheka S, et al. In situ doping of black phosphorus by high-pressure synthesis. Inorg Chem, 2019, 58: 10227–10238
31 Huang Y, Qiao J, He K, et al. Interaction of black phosphorus with oxygen and water. Chem Mater, 2016, 28: 8330–8339
32 Yu Y, Xing B, Yao J, et al. N-type doping of black phosphorus single crystal by tellurium. Nanotechnology, 2020, 31: 315605